Rotating Atomic Quantum Gases with Light-Induced Azimuthal Gauge Potentials and the Observation of the Hess-Fairbank Effect

P.-K. Chen,[1] L.-R. Liu,[1] M.-J. Tsai,[1] N.-C. Chiu,[1] Y. Kawaguchi,[2] S.-K. Yip,[1,3,4] M.-S. Chang,[1] and Y.-J. Lin[1,*]
[1]*Institute of Atomic and Molecular Sciences, Academia Sinica, Taipei 10617, Taiwan*
[2]*Department of Applied Physics, Nagoya University, Nagoya 464-8603, Japan*
[3]*Institute of Physics, Academia Sinica, Taipei 11529, Taiwan*
[4]*National Center for Theoretical Sciences, Hsinchu 300, Taiwan*

(Received 2 August 2018; published 18 December 2018)

We demonstrate synthetic azimuthal gauge potentials for Bose-Einstein condensates from engineering atom-light couplings. The gauge potential is created by adiabatically loading the condensate into the lowest energy Raman-dressed state, achieving a coreless vortex state. The azimuthal gauge potentials act as effective rotations and are tunable by the Raman coupling and detuning. We characterize the spin textures of the dressed states, in agreements with the theory. The lowest energy dressed state is stable with a 4.5-s half-atom-number-fraction lifetime. In addition, we exploit the azimuthal gauge potential to demonstrate the Hess-Fairbank effect, the analogue of Meissner effect in superconductors. The atoms in the absolute ground state has a zero quasiangular momentum and transits into a polar-core vortex when the synthetic magnetic flux is tuned to exceed a critical value. Our demonstration serves as a paradigm to create topological excitations by tailoring atom-light interactions where both types of SO(3) vortices in the $|\langle\vec{F}\rangle| = 1$ manifold, coreless vortices and polar-core vortices, are created in our experiment. The gauge field in the stationary Hamiltonian opens a path to investigating rotation properties of atomic superfluids under thermal equilibrium.

DOI: 10.1103/PhysRevLett.121.250401

Synthetic gauge fields for ultracold neutral atoms [1–9] marked one of the milestones toward creating topological quantum matters and exploring novel quantum phenomenon. Among various implementations, the optical Raman coupling scheme is to couple different internal spin states while transferring photon momentum. This leads to the spin-linear-momentum coupling [8–12], which is a type of "general spin-orbit coupling" (SOC), referring to coupling between the atomic spin and the center-of-mass motion of the atoms. Another class of SOC where the atomic spin is coupled to the orbital-angular momentum (OAM) of the atoms [13] has been demonstrated using one Laguerre-Gaussian (LG) Raman beam carrying OAM of light [14]; this is the spin-orbital-angular-momentum coupling (SOAMC) [15–18].

In SOAMC systems, the atoms dressed by LG Raman beams experience azimuthal gauge potentials $\vec{A} = A(r)\mathbf{e}_\phi$, where the azimuthal dispersion is $(\ell - \ell_{\min})^2/2mr^2$ at radial position r and ℓ is the angular momentum. The shifted minimum is $\ell_{\min} = rA(r)$, where $A(r)$ is tunable by the Raman coupling strength $\Omega(r)$ and Raman detuning δ in our experiment. This azimuthal gauge potential is, thus, equivalent to an effective rotation in the stationary Hamiltonian. Rotating atomic quantum gases with such azimuthal gauge potentials differs from those where metastable superflows are created by resonant pulses of Raman LG beams [19,20] or mechanical stirring [21]. In such cases, the spinor wave function is not the eigenstate of the Hamiltonian; therefore the gauge potential is not well defined. Differing from applying Raman pulses in the Rabi-flopping regime, one typically prepares dressed eigenstates with gauge potentials by adiabatically sweeping the detuning (see later text).

The light-induced azimuthal gauge potential can in principle be used to measure superfluid fractions from the spin population imbalance [22]. Superfluid fraction corresponds to a nonclassical rotational inertia (NCRI) [23,24], which is a property of systems under thermal equilibrium, rather than of metastable systems. In Refs. [23,24], NCRI is manifested in the Hess-Fairbank effect [25,26]: with a cylindrical container filled with ^{4}He rotates at a sufficiently low speed, after ^{4}He is cooled below the superfluid transition temperature, the atoms stop rotating and become out of equilibrium with the container. NCRI is also an analog of the Meissner effect in superconductors [23,24].

Some attempts have been made to realize light-induced azimuthal gauge potentials. In Ref. [27], Bose-Einstein condensates (BECs) in a ring trap under LG Raman beams with the OAM transfer between spin states ($|m_F\rangle \to |m_F + 1\rangle$) $\Delta\ell = 3\hbar$ are studied; a lifetime of ~0.1 s of the lowest energy dressed state atoms is reported. $F = 1$ SOAMC BECs are demonstrated in Ref. [14] with the gauge potential $A = 0$, given that the atoms are in the middle-energy dressed state in the $\langle\vec{F}\rangle = 0$ polar phase. In this

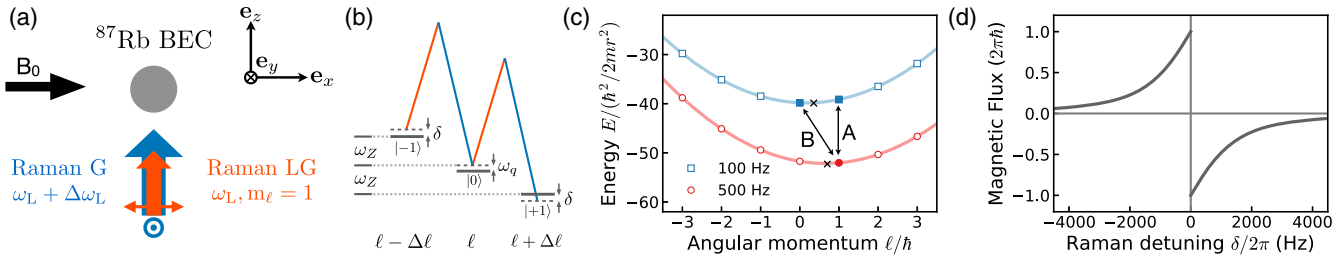

FIG. 1. Experimental schematic and properties of the dressed state. (a) Experiment setup. (b) Level diagram in $F = 1$ manifold. (c) Energy dispersion versus quasiangular momentum ℓ at $r = 2.0$ μm for $\delta/2\pi = 100$ and 500 Hz. "A" indicates $\ell = \hbar$ for both detunings in Fig. 2 data, and "B" indicates $\ell_g = 0, \hbar$ for $\delta/2\pi = 100$ and 500 Hz in Fig. 4, respectively. The x marks indicate the minimum. (d) Synthetic magnetic flux $\Phi^{\pm}_{B^*}$ enclosed by the condensate radius R versus $\delta/2\pi$.

Letter, we present the first experimental realization of such azimuthal gauge potential ($A \neq 0$) with SOAMC BECs in the lowest energy dressed state.

SOAMC BECs can be implemented with an atom-light coupling $\vec{\Omega}_{\rm eff} \cdot \vec{F}$ where the direction of $\vec{\Omega}_{\rm eff}$ winds by a multiple of 2π as the azimuthal angle ϕ increases from 0 to 2π. Here, $\vec{\Omega}_{\rm eff}$ is a light-induced effective magnetic field [8] typically realized by LG Raman beams [14] and $\vec{F}$ is the atomic spin. Topological excitations in spinor BECs, where the rich variety of order parameters accommodates various types of topological defects [28,29], can be created by versatile design of $\vec{\Omega}_{\rm eff}$. This is analogous to the works using spin rotation with real magnetic fields $\vec{B}$ with the Hamiltonian term $\vec{B} \cdot \vec{F}$ [30], where coreless vortices [31], monopoles [32–35], two-dimensional (2D) [36,37] and 3D skyrmions [38], and the geometric Hall effect [39] are demonstrated. Furthermore, 2D skyrmions [40] and spin monopoles [41] with pulses of Raman LG beams are achieved.

In this Letter, we first load a BEC into the lowest energy Raman-dressed state, creating a coreless vortex [28]. Here one Raman beam is LG and carries OAM. The dressed atoms experience azimuthal gauge potentials as effective rotations, which we exploit to demonstrate the Hess-Fairbank effect. When the synthetic magnetic flux arising from the effective rotation is below a critical value, the dressed atoms in the absolute ground state in the thermal equilibrium have zero quasiangular momentum $\ell^{\pm}$ [see later texts and Eq. (4)], being a coreless vortex. Above the critical flux, a polar-core vortex [28,42,43] with nonzero $\ell^{\pm} = \mp\hbar$ is achieved. We demonstrate the capability to create both types of SO(3) vortices [28,29], the $\mathbb{Z}_2 = 0$ coreless vortex and $\mathbb{Z}_2 = 1$ polar-core vortex [see the schematic drawing in Fig. 4(b)] in a unified and controlled scheme. This opens a path for creating topological excitations by tailoring atom-light interactions.

For atoms under sufficiently large $\vec{\Omega}_{\rm eff} \cdot \vec{F}$ such that the motional kinetic energy $-(\hbar^2/2m)\nabla^2$ is negligible, the energy eigenstates of the overall Hamiltonian are well approximated by the eigenstates $|\xi_n\rangle$ of $\vec{\Omega}_{\rm eff} \cdot \vec{F}$. Under this approximation, the atom's spinor wave function follows the local dressed eigenstate $|\xi_n\rangle$, whose quantization axis is along $\vec{\Omega}_{\rm eff} = \Omega(r)\cos\phi \mathbf{e}_x - \Omega(r)\sin\phi \mathbf{e}_y + \delta \mathbf{e}_z$ given by our Raman beams. The state of dressed atoms is $\langle \vec{r}|\Psi\rangle = \varphi_n(\vec{r})|\xi_n(\vec{r})\rangle$, where φ_n is the external part and $|\xi_n\rangle$ is the normalized spin part of the wave function. $|\varphi_n| = \sqrt{n_a}$ where n_a is the density. The effective Hamiltonian for atoms projected to $|\xi_n\rangle$ [14], which governs the evolution of φ_n, is

$$H^{(n)}_{\rm eff} = \frac{-\hbar^2}{2m}\nabla^2(r,z) + \frac{(L_z - rA_n)^2}{2mr^2} + V(r) + \varepsilon_n + W_n. \tag{1}$$

Here $L_z = -i\hbar\partial_\phi$ is the angular momentum operator for φ_n with the eigenvalue ℓ, and $A_n(r) = (i\hbar/r)\langle\xi_n|\partial_\phi\xi_n\rangle$ is the azimuthal gauge potential. $V(r)$ is the spin-independent trap, $\varepsilon_n = n\sqrt{\Omega(r)^2 + \delta^2}$ is the eigenenergy of $\vec{\Omega}_{\rm eff} \cdot \vec{F}$, and $W_n \approx \hbar^2/2mr^2$ is the geometric scalar potential. We label the lowest, middle, and highest energy dressed states as $|\xi_{-1}\rangle, |\xi_0\rangle, |\xi_1\rangle$, respectively. $|\xi_{-1}\rangle$ is given by Euler rotations [44]

$$|\xi_{-1}\rangle = e^{i(\theta+\gamma)}\left(e^{i\phi}\frac{1-\cos\beta}{2}, -\frac{\sin\beta}{\sqrt{2}}, e^{-i\phi}\frac{1+\cos\beta}{2}\right)^T, \tag{2}$$

where $\beta(r) = \tan^{-1}[\Omega(r)/\delta]$ is the polar angle of $\vec{\Omega}_{\rm eff}$, and $\theta + \gamma$ is the phase from a gauge transformation. By choosing $\theta + \gamma = 0$ for all δ, it leads to

$$A_{-1} = (\hbar/r)\cos\beta, \tag{3}$$

where the angular momentum of φ_{-1} is ℓ in this gauge, and ℓ, $\ell \pm \hbar$ are the mechanical angular momenta of the bare spin $|m_F = 0, \pm 1\rangle$ components of the state $\varphi_{-1}|\xi_{-1}\rangle$, respectively. In order to avoid a singularity at $r = 0$ in the synthetic magnetic field $\vec{B}^* = \nabla \times \vec{A}$ [45] as $A_{-1}(r \to 0) \to \pm\hbar/r$ for $\delta > (<)0$, we use alternative gauges with $\theta + \gamma = \pm\phi$, leading to

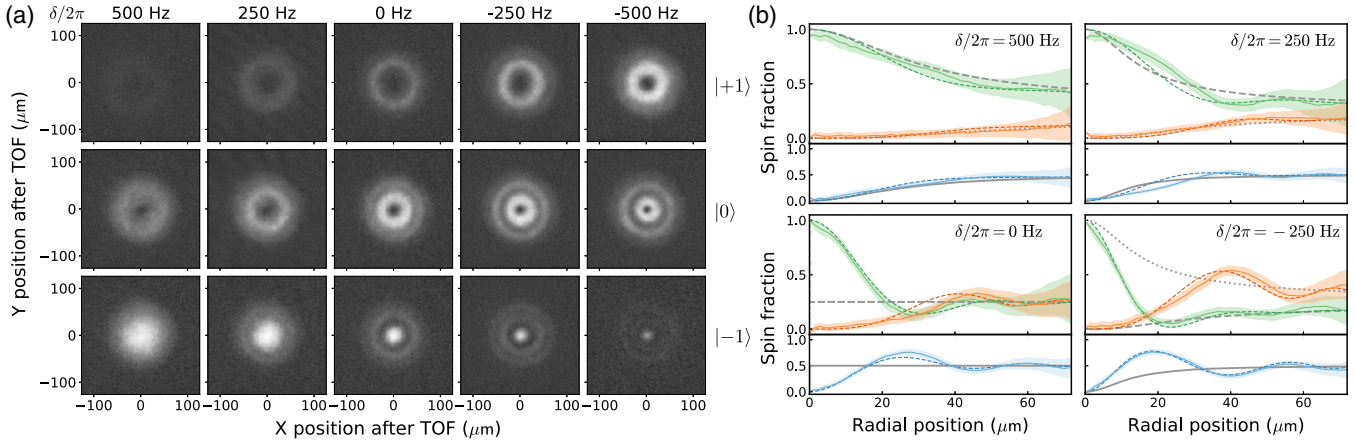

FIG. 2. (a) Absorption images D_{m_F} of the lowest energy dressed state projected onto bare spin $|m_F\rangle$ states with various detuning δ after 24 ms TOF. (b) Experimental spin fractions (solid colored lines) versus the radial position are compared to the spin texture from $|\xi_{-1}\rangle$ (gray lines) and the TOF simulations from TDGPE (dashed colored lines). The green, orange, and blue curves represent the $|-1\rangle$, $|1\rangle$, $|0\rangle$ components, respectively, where the shaded area indicates the standard deviation along $\mathbf{e}_\phi$. The *in situ* spin textures from Eq. (5) after a magnification of $r \to r/13.0$ after TOF [14,46] are shown as gray-dashed, -dotted, and -solid lines for $|-1\rangle$, $|1\rangle$, $|0\rangle$ states.

$$A_{-1}^{\pm} = \frac{\hbar}{r}(\cos\beta \mp 1), \qquad \ell^{\pm} = \ell \mp \hbar, \tag{4}$$

for $\delta > (<)0$, where $\ell^{\pm}$ is the angular momentum of the external wave function $\varphi_{-1}^{\pm}$ in these gauges. Note that the mechanical angular momentum $\ell - rA_{-1} = \ell^{\pm} - rA_{-1}^{\pm}$ is gauge invariant.

Consider atoms in the lowest energy dressed state $|\xi_{-1}\rangle$ prepared by loading a ground state BEC in $|m_F = -1\rangle$ with a Thomas-Fermi (TF) wave function $\varphi_{\mathrm{TF}} = \sqrt{n_{\mathrm{TF}}}$, where $\langle\vec{r}|\Psi\rangle_{t=0} = \varphi_{\mathrm{TF}}(0,0,1)^T$. The atoms are loaded to $|\xi_{-1}\rangle$ as

$$\langle\vec{r}|\Psi\rangle = \varphi_{\mathrm{TF}}\left(e^{i2\phi}\frac{1-\cos\beta}{2}, -e^{i\phi}\frac{\sin\beta}{\sqrt{2}}, \frac{1+\cos\beta}{2}\right)^T, \tag{5}$$

where the phase winding of the $m_F = -1$ component remains zero during loading, and the potential $V(r)$ is cylindrically symmetric. Equation (5) has $\ell = \hbar$ using the gauge in Eq. (3), as shown in our data in Fig. 2. The atom's spinor wave function follows $|\xi_{-1}\rangle$ only at $r \gtrsim r_c$ due to the vanishing intensity of LG beam at $r = 0$, where r_c is the adiabatic radius. At $r \gtrsim r_c$, the radial kinetic energy is negligible and for sufficiently slow $\dot{\delta}$ adiabatic loading is achieved.

We perform 3D time-dependent Gross-Pitaevskii equation (TDGPE) calculations to simulate the loading of a BEC from $|m_F = -1\rangle$ into the dressed state $|\xi_{-1}\rangle$. We also solve the absolute ground state using imaginary time propagations at given $\Omega(r)$ and δ.

Our experiment begins with $N \approx 1.2 \times 10^5$ atoms in a ^{87}Rb BEC in the $|F = 1, m_F = -1\rangle$ state in a crossed dipole trap. The TF radius of the condensate is $R \approx 6.2$ μm along $\mathbf{e}_r$. With a bias magnetic field B_0 along $\mathbf{e}_x$, the atoms experience a linear Zeeman shift $\omega_Z/2\pi = 0.57$ MHz and a quadratic Zeeman shift $\hbar\omega_q\hat{F}_z^2$ with $\omega_q/2\pi = 50$ Hz. A Gaussian (G) Raman beam and a Laguerre-Gaussian (LG) Raman beam with phase winding $m_\ell = 1$ copropagate along $\mathbf{e}_z$, coupling atoms in the $F = 1$ manifold and transferring OAM of $\Delta\ell = \hbar$ to the atoms [Fig. 1(b)]. The two Raman laser beams have wavelengths $\lambda = 790$ nm with a frequency difference $\Delta\omega_L$ and a Raman detuning $\delta = \Delta\omega_L - \omega_Z$ [Figs. 1(a) and 1(b)]. We adiabatically load the BEC into the lowest energy dressed state $|\xi_{-1}\rangle$ with final Raman coupling strength $\Omega(r) = \Omega_M\sqrt{e}(r/r_M)e^{-r^2/2r_M^2}$. Here, $\Omega_M/2\pi = 3.0$ kHz and $r_M = 17$ μm is the peak intensity radius.

The adiabatic loading is achieved by first turning on $\Omega(r)$ in 7 ms while holding the detuning at $\delta/2\pi = \delta_f/2\pi + 1.25$ kHz. Next, we sweep the detuning to the final value δ_f in 7 ms where -500 Hz $< \delta_f/2\pi <$ 500 Hz. After preparing the atoms in the dressed state and holding for a time t_h, we probe the atoms by switching off the Raman beams and dipole trap simultaneously. After a 24-ms time-of-flight (TOF) with all $|m_F\rangle$ components expanding together, we take absorption images along $\mathbf{e}_z$ for each m_F states. Images with different final detuning δ and $t_h = 1$ ms are shown in Fig. 2(a). For $\delta > 0$, the $|m_F = -1\rangle$ component has no hole, and $|0\rangle$ carries a smaller hole than that of $|1\rangle$, consistent with the fact that $|-1\rangle$, $|0\rangle$, $|1\rangle$ have angular momenta of 0, $\hbar$, $2\hbar$, respectively. The radial cross sections of the spin texture $D_{m_F}/(D_1 + D_0 + D_{-1})$ are shown [Fig. 2(b)], which average over the azimuthal angles. Here, D_{m_F} is the optical density of $|m_F\rangle$. We compare these spin textures with the local dressed state $|\xi_{-1}\rangle$ in Eq. (5) and TOF simulations from TDGPE. The TDGPE simulation gives an $r_c \approx 1.8$ μm at $\delta = 0$, corresponding to the spin texture agreeing with Eq. (5) at $r_{\mathrm{TOF}} \gtrsim 23$ μm.

We further study the stability of the lowest energy dressed state as we hold the Raman field for a variable

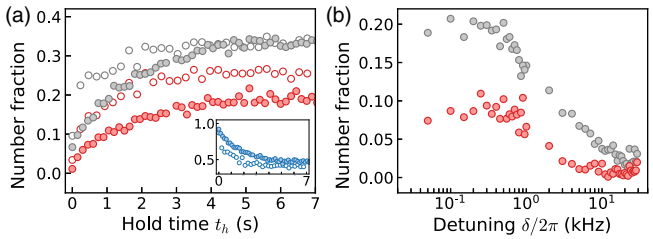

FIG. 3. Stability of lowest energy dressed state $|\xi_{-1}\rangle$, shown as the number fraction in the excited dressed states $|\xi_0\rangle$ (gray circles) and $|\xi_1\rangle$ (red circles): (a) Versus hold time t_h at $\delta = 0$ for $\Omega_M/2\pi = 3.0$ kHz (solid circles) and 1.5 kHz (open circles). Inset shows the number fraction in $|\xi_{-1}\rangle$ versus t_h. (b) Versus detuning with $t_h = 1$ s and $\Omega_M/2\pi = 3.0$ kHz.

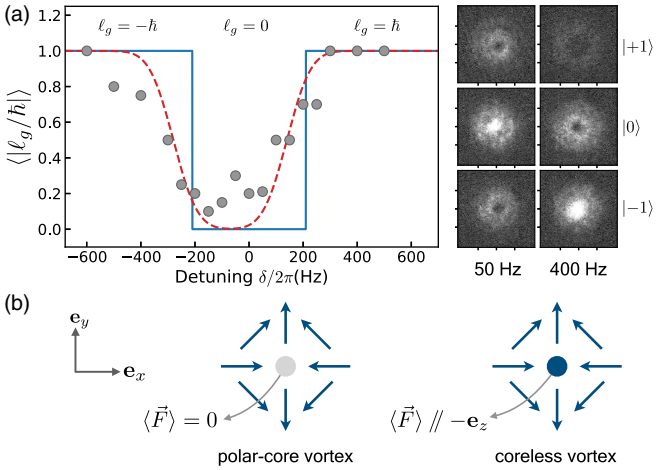

FIG. 4. (a) Transition between $\ell = 0$ and $\ell = \pm\hbar$ states in the ground state. The measured average of magnitude of the quasiangular momentum of the ground state atoms $\langle|\ell_g|\rangle$ versus detuning $\delta/2\pi$ (circles) with $t_{h1} \approx 0.2$ s. At small (large) $|\delta|$ the ground state has $|\ell_g| = 0$ ($\hbar$). Examples at $\delta/2\pi = 50$ and 400 Hz are shown with the dressed states' bare spin components taken after TOF. The calculation for the ideal case (solid line) and a simulation including detuning noise in the experiment (dashed line) are displayed; see text. (b) Schematic drawing of the spin textures at $\delta > 0$, where the arrows show the direction of the transverse spin ($\langle F_x\rangle$, $\langle F_y\rangle$).

time t_h. With a deloading procedure [14] which maps the dressed states $|\xi_{-1}\rangle$, $|\xi_0\rangle$, $|\xi_1\rangle$ back to the bare spin states $|-1\rangle, |0\rangle, |+1\rangle$, we measure the population in $|\xi_n\rangle$ versus t_h. We take images along $\mathbf{e}_y$ after 14-ms TOF with Stern-Gerlach gradient at a variable δ with a t_h up to 7.0 s. Figure 3(a) shows the atom number fraction in $|\xi_n\rangle$ over the total number $|\xi_{-1}\rangle + |\xi_0\rangle + |\xi_1\rangle$ at $\delta = 0$ versus t_h. The atoms slowly populate the excited dressed states $|\xi_0\rangle$ and $|\xi_1\rangle$, and the initial rates increase as the peak Raman coupling is reduced from $\Omega_M/2\pi = 3.0$ to 1.5 kHz. The lifetime of atom number fraction in $|\xi_{-1}\rangle$ dropping to 50% is 4.5 s (1.5 s) for $\Omega_M/2\pi = 3.0(1.5)$ kHz. Figure 3(b) displays the atom number fraction versus detuning at $t_h = 1$ s and $\Omega_M/2\pi = 3.0$ kHz, where the population transfer rates decrease with increasing $|\delta|$. The results suggest the population transfer rate into excited states increases with a reduction of energy gap $\approx\sqrt{\Omega(r)^2 + \delta^2}$, which can be explained by the effects of thermal atoms. Our estimated temperature $T \gtrsim 50$ nK $\approx h \times 1$ kHz$/k_B$ is comparable to the energy gap in the experiment.

Finally, we demonstrate the Hess-Fairbank effect by studying the absolute ground state of dressed atoms in the gauge fields. We begin with thermal atoms right above the BEC transition temperature, load to the lowest energy dressed state with detuning δ, and evaporatively cool the atoms to BEC. After a hold time t_{h1} for free evaporation, we probe the atoms after a 24-ms TOF. We note that there is a different, but related experiment [47], where thermal bosonic atoms are evaporatively spun up and cooled to reach condensation [48].

Similar to the Meissner effect, we tune the synthetic magnetic flux via the detuning δ and observe the atoms in the absolute ground state transit from having one quantum number to another. Gross-Pitaevskii equation simulations show that the ground states are coreless vortices with $\ell_g = \pm\hbar$ at $|\delta|/2\pi > 210$ Hz and are polar-core vortices with $\ell_g = 0$ at $|\delta|/2\pi < 210$ Hz [Fig. 4(a)]; ℓ_g is ℓ of the ground state. We obtain the averaged absolute value of winding number $\langle|\ell_g|\rangle/\hbar$ versus detuning in Fig. 4, by taking TOF images of the bare spin component $|m_F = 0\rangle$, whose mechanical angular momentum is ℓ_g under the gauge in Eq. (3). At each δ we repeat the experiment for 20 times, observing $|m_F = 0\rangle$ has either no hole or a hole, indicating $\ell_g = 0$ or $\ell_g = \pm\hbar$, respectively. Such variations are due to the presence of a root-mean-square (rms) detuning noise of $\approx h \times 70$ Hz (as we repeat the experiment with the same t_{h1}, see Supplemental Material [49]) arising from the bias field noise in our setup. The curve $\langle|\ell_g|\rangle$ vs $\delta/2\pi$ is broadened and can become slightly asymmetric at $\pm\delta$ because the detuning can slowly vary during the time when the data are taken. A simulation including a Gaussian-distributed detuning noise of $h \times 70$ Hz rms is plotted in Fig. 4(a), with a center shift of -70 Hz. The observed ground state with small $|\delta|$ has $\langle|\ell_g|\rangle/\hbar \sim 0$, corresponding to $\ell_g = 0$ if there were no detuning noise. Figure 4(a) shows the image of the $\ell_g = 0$ ($\ell_g = \hbar$) dressed state at $\delta/2\pi = 50(400)$ Hz; the spin textures are schematically drawn in Fig. 4(b).

We compare our dressed atoms under gauge-induced rotations to BECs under mechanical rotations [50–52]. In Refs. [50–52], Bose condensation is followed by mechanical stirring. The observed critical rotational angular frequency for single-vortex nucleation is related to dynamical instabilities and is larger than the critical value ω_c for the thermodynamic ground state to possess a single vortex. By contrast, in our demonstration of the Hess-Fairbank effect, the thermal atoms are subjected to the effective rotation and then cooled to BEC in the thermodynamic ground state.

Using the gauges in Eq. (4), the synthetic magnetic flux enclosed by the BEC's radius R is $\Phi_{B^*}^{\pm} = h[\cos\beta(R) \mp 1]$. Figure 1(d) shows $|\Phi_{B^*}^{\pm}|$ approaches zero at large $|\delta|$, and $\vec{B}^*$ is along $-(+)\mathbf{e}_z$ at $\delta > (<)0$. Thus, our system is analogous to the transition from zero to single-vortex ground state in rotating BECs as the following: $\ell^+ = 0 \to \ell^+ = -\hbar$ (i.e., $\ell = \hbar \to \ell = 0$) under $\Phi_{B^*}^{+} < 0$. And similarly for $\ell^- = 0 \to \ell^- = \hbar$ (i.e., $\ell = -\hbar \to \ell = 0$) under $\Phi_{B^*}^{-} > 0$. At the transition of $\delta/2\pi = \pm 210$ Hz, $|\Phi_{B^*}^{\pm}| = 0.8h$ is smaller than the critical effective flux Φ_{mech} for mechanically rotating BECs. The flux is $\Phi_{\mathrm{mech}} = 2\pi m\omega R^2 = h(\omega/\omega_c)\ln(R/r_v)$, where ω is the angular frequency, $\omega_c = \hbar/(mR^2)\ln(R/r_v)$ [53], and r_v is the vortex core size. Thus, the critical flux is $\Phi_{\mathrm{mech}}/h > 1$, whereas the critical flux for our dressed state is $|\Phi_{B^*}^{\pm}|/h < 1$. This is due to the different form of $A(r)$ between our dressed atoms and the mechanically rotating BECs (with symmetric gauge); see Supplemental Material [49] and a similar calculation in Ref. [54].

In conclusion, we demonstrate Raman-coupling-induced azimuthal gauge potentials. They act as effective rotations which we exploit to show Hess-Fairbank effect for the cold atoms. This Letter paves the way to probe atomic superfluids with effective rotations, which can achieve a stationary Hamiltonian and thermal equilibrium. This scheme circumvents the issues from imperfect cylindrical symmetries in mechanical rotations.

We thank W. D. Phillips, C. Chin, and K.-Y. Lin for useful discussions, and Y.-C. Chen and J.-P. Wang for critical readings of our manuscript. Y.-J. L acknowledges the support of Career Development Award in Academia Sinica, Grant No. 102-CDA-M03. S.-K. Y. was supported by MOST Grants No. 104-2112-M-001-006-MY3 and No. 107-2112-M-001-035-MY3. Y. K. was supported by JSPS KAKENHI Grant No. JP15K17726. M.-S. C. and M.-J. T. were supported by MOST Grant No. 106-2112-M-001-033.

Note added.—We noticed a recent work [55] on pseudospin 1/2 SOAMC BECs. They reported observations similar to our demonstration of Hess-Fairbank effect. Our Letter focuses on the perspective of effective rotations enabled by light-induced azimuthal gauge potentials and characterizing topological spin textures.

*linyj@gate.sinica.edu.tw

[1] Y.-J. Lin, R. L. Compton, A. R. Perry, W. D. Phillips, J. V. Porto, and I. B. Spielman, Phys. Rev. Lett. **102**, 130401 (2009).
[2] M. Aidelsburger, M. Atala, M. Lohse, J. T. Barreiro, B. Paredes, and I. Bloch, Phys. Rev. Lett. **111**, 185301 (2013).
[3] H. Miyake, G. A. Siviloglou, C. J. Kennedy, W. C. Burton, and W. Ketterle, Phys. Rev. Lett. **111**, 185302 (2013).
[4] J. Struck, C. Ölschläger, M. Weinberg, P. Hauke, J. Simonet, A. Eckardt, M. Lewenstein, K. Sengstock, and P. Windpassinger, Phys. Rev. Lett. **108**, 225304 (2012).
[5] C. V. Parker, L.-C. Ha, and C. Chin, Nat. Phys. **9**, 769 (2013).
[6] G. Jotzu, M. Messer, R. Desbuquois, M. Lebrat, T. Uehlinger, D. Greif, and T. Esslinger, Nature (London) **515**, 237 (2014).
[7] J. Dalibard, F. Gerbier, and G. Juzeliūnas, and P. Öhberg, Rev. Mod. Phys. **83**, 1523 (2011).
[8] N. Goldman, G. Juzeliunas, P. Öhberg, and I. B. Spielman, Rep. Prog. Phys. **77**, 126401 (2014).
[9] H. Zhai, Rep. Prog. Phys. **78**, 026001 (2015).
[10] Y. J. Lin, K. Jimenez-Garcia, and I. B. Spielman, Nature (London) **471**, 83 (2011).
[11] Z. Wu, L. Zhang, W. Sun, X.-T. Xu, B.-Z. Wang, S.-C. Ji, Y. Deng, S. Chen, X.-J. Liu, and J.-W. Pan, Science **354**, 83 (2016).
[12] L. Huang, Z. Meng, P. Wang, P. Peng, S.-L. Zhang, L. Chen, D. Li, Q. Zhou, and J. Zhang, Nat. Phys. **12**, 540 (2016).
[13] G. Juzeliunas, P. Öhberg, J. Ruseckas, and A. Klein, Phys. Rev. A **71**, 053614 (2005).
[14] H.-R. Chen, K.-Y. Lin, P.-K. Chen, N.-C. Chiu, J.-B. Wang, C.-A. Chen, P.-P. Huang, S.-K. Yip, Y. Kawaguchi, and Y.-J. Lin, Phys. Rev. Lett. **121**, 113204 (2018).
[15] C. Qu, K. Sun, and C. Zhang, Phys. Rev. A **91**, 053630 (2015).
[16] M. DeMarco and H. Pu, Phys. Rev. A **91**, 033630 (2015).
[17] Y.-X. Hu, C. Miniatura, and B. Grémaud, Phys. Rev. A **92**, 033615 (2015).
[18] L. Chen, H. Pu, and Y. Zhang, Phys. Rev. A **93**, 013629 (2016).
[19] A. Ramanathan, K. C. Wright, S. R. Muniz, M. Zelan, W. T. Hill, C. J. Lobb, K. Helmerson, W. D. Phillips, and G. K. Campbell, Phys. Rev. Lett. **106**, 130401 (2011).
[20] S. Beattie, S. Moulder, R. J. Fletcher, and Z. Hadzibabic, Phys. Rev. Lett. **110**, 025301 (2013).
[21] K. C. Wright, R. B. Blakestad, C. J. Lobb, W. D. Phillips, and G. K. Campbell, Phys. Rev. Lett. **110**, 025302 (2013).
[22] N. R. Cooper and Z. Hadzibabic, Phys. Rev. Lett. **104**, 030401 (2010).
[23] A. J. Leggett, Rev. Mod. Phys. **71**, S318 (1999).
[24] A. J. Leggett, Rev. Mod. Phys. **73**, 307 (2001).
[25] G. B. Hess and W. M. Fairbank, Phys. Rev. Lett. **19**, 216 (1967).
[26] R. Ishiguro, O. Ishikawa, M. Yamashita, Y. Sasaki, K. Fukuda, M. Kubota, H. Ishimoto, R. E. Packard, T. Takagi, T. Ohmi *et al.*, Phys. Rev. Lett. **93**, 125301 (2004).
[27] S. Moulder, Ph. D. thesis, University of Cambridge, 2013.
[28] Y. Kawaguchi and M. Ueda, Phys. Rep. **520**, 253 (2012).
[29] M. Ueda, Rep. Prog. Phys. **77**, 122401 (2014).
[30] T. Isoshima, M. Nakahara, T. Ohmi, and K. Machida, Phys. Rev. A **61**, 063610 (2000).
[31] A. E. Leanhardt, Y. Shin, D. Kielpinski, D. E. Pritchard, and W. Ketterle, Phys. Rev. Lett. **90**, 140403 (2003).
[32] M. W. Ray, E. Ruokokoski, S. Kandel, M. Möttönen, and D. S. Hall, Nature (London) **505**, 657 (2014).

[33] M. W. Ray, E. Ruokokoski, K. Tiurev, M. Möttönen, and D. S. Hall, Science **348**, 544 (2015).
[34] D. S. Hall, M. W. Ray, K. Tiurev, E. Ruokokoski, A. H. Gheorghe, and M. Möttönen, Nat. Phys. **12**, 478 (2016).
[35] T. Ollikainen, K. Tiurev, A. Blinova, W. Lee, D. S. Hall, and M. Möttönen, Phys. Rev. X **7**, 021023 (2017).
[36] J.-Y. Choi, W. J. Kwon, and Y.-I. Shin, Phys. Rev. Lett. **108**, 035301 (2012).
[37] J.-Y. Choi, W. J. Kwon, M. Lee, H. Jeong, K. An, and Y.-i. Shin, New J. Phys. **14**, 053013 (2012).
[38] W. Lee, A. H. Gheorghe, K. Tiurev, T. Ollikainen, M. Möttönen, and D. S. Hall, Sci. Adv. **4**, eaao3820 (2018).
[39] J.-Y. Choi, S. Kang, S. W. Seo, W. J. Kwon, and Y.-i. Shin, Phys. Rev. Lett. **111**, 245301 (2013).
[40] L. S. Leslie, A. Hansen, K. C. Wright, B. M. Deutsch, and N. P. Bigelow, Phys. Rev. Lett. **103**, 250401 (2009).
[41] A. Hansen, Ph.D. thesis, University of Rochester, 2016.
[42] T. Isoshima, K. Machida, and T. Ohmi, J. Phys. Soc. Jpn. **70**, 1604 (2001).
[43] L. E. Sadler, J. M. Higbie, S. R. Leslie, M. Vengalattore, and D. M. Stamper-Kurn, Nature (London) **443**, 312 (2006).
[44] T.-L. Ho, Phys. Rev. Lett. **81**, 742 (1998).
[45] T.-L. Ho and V. B. Shenoy, Phys. Rev. Lett. **77**, 2595 (1996).
[46] Y. Castin and R. Dum, Phys. Rev. Lett. **77**, 5315 (1996).
[47] P. C. Haljan, I. Coddington, P. Engels, and E. A. Cornell, Phys. Rev. Lett. **87**, 210403 (2001).
[48] In Ref. [47], they study vortex nucleation into a BEC in the environment of rotating thermal atoms.
[49] See Supplemental Material at http://link.aps.org/supplemental/10.1103/PhysRevLett.121.250401 for TDGPE simulations, synthetic magnetic flux of dressed atoms, experimental setup and procedures, and data analysis.
[50] K. W. Madison, F. Chevy, V. Bretin, and J. Dalibard, Phys. Rev. Lett. **86**, 4443 (2001).
[51] J. R. Abo-Shaeer, C. Raman, J. M. Vogels, and W. Ketterle, Science **292**, 476 (2001).
[52] E. Hodby, G. Hechenblaikner, S. A. Hopkins, O. M. Maragò, and C. J. Foot, Phys. Rev. Lett. **88**, 010405 (2001).
[53] E. Lundh, C. J. Pethick, and H. Smith, Phys. Rev. A **55**, 2126 (1997).
[54] G. Juzeliunas and P. Öhberg, Opt. Spectrosc. **99**, 357 (2005).
[55] D. Zhang, T. Gao, P. Zou, L. Kong, R. Li, X. Shen, X.-L. Chen, S.-G. Peng, M. Zhan, H. Pu *et al.*, arXiv:1806.06263.